

Behaviour of axially compressed CTHST stub columns with inner spiral stirrup

You-Fu Yang[a,*], Yu-Qin Zhang[a], Feng Fu[b]

[a] *State Key Laboratory of Coastal and Offshore Engineering, Dalian University of Technology, Dalian, 116024, China*
[b] *Department of Engineering, School of Science and Technology, City University of London, Northampton Square, London, UK*

Abstract: In this paper, a new type of concrete-filled thin-walled high-strength steel tube (CTHST) columns with inner spiral stirrup is proposed. This new type of columns provides dual constraints to the concrete core by both outer steel tube and inner spiral stirrup. To explore the structural performance of this new type of composite members, a pilot study into stub columns under axial compression was carried out. A total of 16 axially compressed specimens, 8 in circular section and 8 in square section, were tested with the various volumetric stirrup ratio (ρ, from 0 to 2.4%) and yield strength of steel tube (f_{yt}, 571.2 MPa and 648.9 MPa). The experimental results show that, the inner spiral stirrup has little impact on the overall failure pattern of each component of the specimens, but controls the horizontal angle of the failure plane, and the capacity, composite elastic modulus and ductility coefficient of the specimens increase as ρ and f_{yt} increase. In addition, a nonlinear finite element (FE) model was established, and the representative mechanism of axially compressed CTHST stub columns with inner spiral stirrup under different ρ was further studied by the verified FE model. Finally, a calculation method to predict the capacity of the new composite members was developed, which considers the strength improvement of stirrup confined concrete. This method provided an accurate prediction of the capacity of axially compressed CTHST stub columns with inner spiral stirrup.

Key Words: CTHST stub columns; Spiral stirrup; Axial compression; Tests; FE model; Simplified equations

*Corresponding author. Tel.: 86-411-8470 8510; Fax: 86-411-8467 4141.
E–mail address: youfuyang@163.com (Dr. You-Fu Yang).

1. Introduction

Concrete-filled steel tube (CFST) members have the characteristics of high strength, good ductility and toughness, convenient construction, good fire resistance, etc. In the past several decades, CFST has been widely used in engineering practice, and a number of design specifications have also been issued across the world [1-3]. However, with the rapid development of social economy and urbanization, modern engineering structures start to be featured in long-span, heavy-duty and towering while in harsh environmental conditions, and conventional CFST is difficult to satisfy these changes. As a result, the idea of combining conventional CFST and reinforced concrete to form reinforced CFST was proposed by the researchers, and the usage of reinforced CFST can improve the mechanical properties of conventional CFST members while having little cost increase [4-11]. Fig. 1 shows the typical cross-section of the reinforced CFST presented in the literature. Generally, the concept of the reinforced CFST was first considered from the perspective of improving the fire resistance of conventional CFST columns [4, 5], and usually the contribution of reinforcement to the bearing capacity was ignored. In recent years, more researchers studied the structural behaviour and design methods of various reinforced CFST members aiming to improve the bearing capacity, stiffness and ductility of conventional CFST members [6-11].

It is noted that, in recent years, high strength and high-performance structural materials have gradually been developed, such as the ultra-high strength steel, weather-resistant steel and ultra-high performance concrete [12-14]. Meanwhile, in practice, the use of high-strength/performance steel can greatly reduce the amount of steel and improve the ability to resist disasters and environmental effects, and the use of high-strength/performance concrete can effectively reduce the cross-sectional area and the self-weight [3, 15-17]. However, local buckling of thin-walled high-strength steel tube becomes worse and the brittleness of high-strength concrete increases with the increase of materials' strength, which results in a weak interaction between steel tube to concrete core within common steel ratio scope of the CFST members. To tackle above issues, the authors proposed a new type of composite member based on the reinforced CFST shown in Fig. 1, concrete-filled thin-walled high-strength steel tube (CTHST) with inner spiral stirrup, as schematically demonstrated in Fig. 2, where the inner spiral stirrup is directly in contact with the inner wall of the steel tube. This configuration ensures that the concrete core of CTHST with inner spiral stirrup is under the dual constraints from both high-strength steel tube and spiral stirrup, which makes CTHST with inner spiral stirrup have the characteristics of high strength, good ductility and excellent energy consumption, and more suitable for engineering structures in high intensity earthquake area.

During fabrication of CTHST member with inner spiral stirrup, the spiral stirrup can be processed in advance by special operating platform while keeping the outer diameter of spiral stirrup ring slightly smaller than the inner diameter/width of the steel tube, and then be slided into the steel tube with its two ends welded to the corresponding ends of the steel tube. Moreover, when the existing and new segments are connected, the welding position between the spiral stirrup in two segments and the steel tube should be overlapped to ensure continuity of spiral stirrup. Finally, after the completion of the steel tube docking (welding), concrete is poured into the steel tube to complete the construction of the composite member. Generally, the processing and welding time of spiral stirrup has moderate impact on the construction period of new composite member, while the mechanical properties of new composite member are expected to be greatly improved. Compared with the reinforced CFST with both longitudinal bars and stirrup(s), the CTHST member with inner spiral stirrup can avoid the binding and extension of the longitudinal bars, and the spiral stirrup can confine the concrete core to the maximum extent. Similar composite members with square section have been presented in [6] and [10]. The cross-section of the specimens in [6] was the same as Fig. 2(b) in this paper, but all materials used were of ordinary strength grade. In addition, the reinforcement and concrete of the specimens in [10] were of high strength grade, and there was a small gap between spiral stirrup and inner wall of the steel tube.

It can be concluded that, besides the parameters of conventional CFST [1], the volumetric stirrup ratio (ρ) is the key parameter affecting the behaviour of CTHST members with inner spiral stirrup. The definition of ρ is as follows:

$$\rho = \frac{V_{\mathrm{sti}}}{V_{\mathrm{nc}}} \tag{1}$$

where, V_{sti} and V_{nc} are the volume of spiral stirrup and the volume enclosed by inner wall of the steel tube under the same member height respectively, and can be respectively determined by the following equations:

$$V_{\mathrm{sti}} = A_{\mathrm{s,s}} \cdot (H/s + 1) \cdot \sqrt{\pi^2 (D_{\mathrm{s}} - d_{\mathrm{s}})^2 + s^2} \tag{2}$$

$$V_{\mathrm{nc}} = \begin{cases} \pi (D/2 - t)^2 \cdot H & \text{(Circular member)} \\ (D - 2t)^2 \cdot H & \text{(Square member)} \end{cases} \tag{3}$$

in which, $A_{\mathrm{s,s}}$ is the cross-sectional area of the stirrup, H is height of the member, s is the spacing of the spiral stirrup, D_{s} is the outer diameter of the spiral along the cross-section of the member, d_{s} is the nominal diameter of the stirrup, D is the outside diameter (width) of circular (square) steel tube, and t is the wall thickness of the steel tube.

Currently, the research on spiral stirrup reinforced CFST is insufficient and premature, and no research has been done towards the new type CTHST columns with inner spiral stirrup proposed in this paper. Therefore, it is necessary to carry out the relevant studies to understand the structural performance of such new composite members and promote their engineering application. The objective of the paper is thus to experimentally and numerically assess the axial compressive performance of CTHST stub columns with inner spiral stirrup. Tests of 16 specimens were carried out to evaluate the effect of volumetric stirrup ratio and yield strength of steel tube on the failure pattern, load versus displacement (strain) curves, capacity, composite elastic modulus and ductility coefficient of axially compressed CTHST stub columns with inner spiral stirrup, and further finite element (FE) model was proved to be effective for simulating the behaviour of such composite columns. Moreover, the applicability of a proposed method in predicting capacity of new composite members was assessed by contrast between the predicted and measured results.

2. Experimental investigation

2.1. Details of the specimens

Sixteen stub column specimens, containing eight with circular section and eight with square section, were designed and manufactured. The height (H) of all specimens is 3 times the cross-sectional diameter or width (D). The tests were primarily considered to assess the impact of ρ (from 0 to 2.4%) and yield strength of steel tube f_{yt} (571.2 MPa and 648.9 MPa) on the performance of axially compressed CTHST stub columns with inner spiral stirrup.

Table 1 presents the details of the specimens, where α_n is the nominal cross-sectional steel ratio equal to the ratio of the area of the steel tube to that enclosed by the tube inner wall, f_{ys} is the yield strength of the stirrup, f_{cu} is the cubic compressive strength of concrete while conducting the tests of composite specimens, $E_{sc,e}$ and $N_{u,e}$ are the experimental composite elastic modulus and capacity of the specimens, respectively, and $E_{sc,fe}$ and $N_{u,fe}$ are the predicted composite elastic modulus and capacity based on the FE model described later, respectively. In Table 1, the first portion in label denotes the cross-sectional shape (C=circular, and S=square) and the yield strength of the steel tube (I for f_{yt}=571.2 MPa, and II for f_{yt}=648.9 MPa), while the second portion in label, if any, indicates the spacing of inner spiral stirrup.

Two kinds of high-strength steel sheet were chosen for fabricating the outer tubes. Circular tubes were coiled from the pre-cut rectangular steel sheet according to the design sizes, and each circular tube had one straight butt weld. Square tubes were welded by two cold-formed unequal U-shaped steel profiles, and each square tube had two straight butt welds. After the steel tubes finished, the spiral stirrup with the designed spacing was slided into the steel tube and welded to both ends of the steel tube. The welding was under strict quality control to guarantee the effective force transmission. Fig. 3 illustrates the finished outer tube and inner stirrup of the specimens. To facilitate pouring of concrete, one circular/square endplate with diameter/width slightly greater than D was welded to one end of tube, and the concrete was cast into the tube from the end without endplate. After 14 days of concrete curing, the surface of the filled concrete was polished to level with the end of the steel tube to ensure that the steel tube and concrete under dual constraints could simultaneously bear the external loads.

2.2. Material properties

The properties of steel, including high-strength steel for the tubes and deformed rebar for the spiral stirrup, were experimentally obtained from three standard tensile coupons, and the average values are listed in Table 2.

The mix proportions and properties of concrete are given in Table 3, where $f_{\mathrm{cu},28}$ is the compressive strength at 28-day according to axial compression tests of three cubes having width of 150 mm, and E_{c} is the elastic modulus based on axial compression tests of three prisms having side length of 150 mm, 150 mm and 300 mm, respectively. The concrete mix includes: first-grade fly ash, natural river sand, P.O 42.5 cement, crushed limestone coarse aggregate with 5-10 mm particle size, tap water and polycarboxylate type high-range water reducing admixture.

2.3. Test set-up and measurement

Axial compression tests of the specimens were performed on a tester with a capacity of 10000 kN. In order to guarantee that the failure occurs near the half-height region, two adjustable steel sleeves were specially designed to limit the end deformation of the specimens during the loading process, and the height of each sleeve was 100 mm. The applied loads were measured by a load cell placed between the top platen of the tester and the upper plate of top sleeve. In addition, to record the deformation (axial displacements and strains), four displacement transducers (DT) were installed symmetrically on the lower platen of the tester, and longitudinal and transverse strain gauges (SG) were affixed to the tube outer wall at the half-height section of the specimens. For circular specimens, strain gauges were affixed at four points along the circumference with 90 degrees apart, while for square specimens strain gauges were affixed at eight points at the middle and corner of the half-height section, and each point contained one longitudinal SG and one transverse SG. The test set-up and measurement are shown in Fig. 4.

The tests were conducted using displacement control method. Before the load reached the peak value, the displacement increased at a rate of 0.2 mm/min, and after the peak load achieved, the displacement increased at a rate of 1.0 mm/min. When the load borne by the specimens dropped sharply and the deformation increased rapidly, or the load borne by the specimens fell to 60% of the peak load, the tests were terminated.

2.4. Experimental results and discussion

2.4.1. Overall behaviour and failure pattern

The records of the whole loading process showed that, all composite specimens underwent three stages of elastic, elastic-plastic and post-peak, regardless of the existence of inner spiral stirrup. During the elastic stage, there was no evident variation in specimen appearance. During the elastic-plastic stage, the diagonal shear slip lines appeared at the tube of circular specimens and more slip lines emerged as the load approached the peak; however, only initial slight tube bulging occurred to square specimens when the load was close to the peak. During the post-peak stage, for circular specimens, the diagonal shear failure plane throughout concrete section was gradually formed and the dislocation along the failure plane and audible crushing of the concrete core happened with the increase of axial displacement, whilst for square specimens, the initial tube bulging became more and more obvious and there was subsequent tube bulging and noticeable crushing of the concrete core while axial displacement further increased.

Fig. 5 shows the failure pattern of the specimens after completion of the experiments. As can be seen in the pictures, there is no sign of damage within the range of specimen ends covered by the sleeve, showing that the sleeve can effectively prevent the destruction of the specimen ends, and thus the failure occurs near the half-height region of the specimen having more uniform properties. It can be observed from Figs. 5(a) and (b) that, circular specimens exhibit the characteristics of shear failure along diagonal plane (dashed line), and the buckling of the steel tube at the ends of diagonal slip plane is the most serious. In general, with the variation in ρ and f_{yt}, the direction of the diagonal slip plane of circular specimens changes, and the fracture of outer steel tube of three circular specimens exists. These are primmarily caused by the arbitrary distribution of defects in materials and the difficulty in achieving ideal axial compression. It is shown in Figs. 5(c) and (d) that, similar to the previous experimental observations [6][10], the steel tube of square specimens has a major local buckling and 1-2 subsequent minor local buckling, and the local buckling of the steel tube eventually extends to the corner zone; however, the local buckling of tube corner zone becomes slighter with the increase of ρ. Moreover, for the specimens without spiral stirrup, the local buckling of the steel tube almost forms a ring parallel to the horizontal plane, while for the specimens with spiral stirrup the local buckling of the steel tube is usually discontinuous along the circumferential direction and at a certain angle to the horizontal plane (close to the spiral angle of the stirrup). Overall, the parameter f_{yt} possesses a gentle effect on the failure form of square specimens; however, the fracture of the steel tube appears at one corner of two specimens with a lower f_{yt}.

Fig. 6 shows the failure pattern of the concrete core. It can be observed that, generally, there are crushing of concrete core and the deforming of spiral stirrup at the buckling positions of the steel tube, and the fracture of the stirrup (displayed by arrow) can be clearly observed in the concrete crushing area of six specimens with inner spiral stirrup. It should be noted that, the spiral stirrup of the other six specimens with inner spiral stirrup also fractured, which could be judged from the following characteristics of their load-displacement curves. In addition, there is no obvious damage to the concrete core in the regions where the steel tube does not slip and/or buckle.

2.4.2. Load versus deformation curves

The recorded load (N) versus displacement (Δ) curve of the specimens with spiral stirrup and the reference sepcimens without spiral stirrup are displayed in Fig. 7. It is shown that, all $N-\Delta$ curves contains three phases, i.e. elastic, elastic-plastic and post-peak; however, similar to the discovery in previous tests [10], there is more than one sudden drops in the post-peak phase of the $N-\Delta$ curve, indicating that the fracture of the stirrup takes place several times, and the first sudden drop is identified by an inverted triangle. In this study, the peak load obtained from the the recorded $N-\Delta$ curve is considered to be the capacity (N_{ue}) of the specimens, and the results are presented in Table 1. The curves included in Fig. 7 demonstrate that, generally, the initial slope and the displacement corresponding to peak load (Δ_{ue}) of the specimens with spiral stirrup are larger than those of the specimens without spiral stirrup, and the higher the volumetric stirrup ratio (ρ), the larger the initial slope and Δ_{ue} are. Meanwhile, after the peak load attained, the specimens with a higher ρ has a smaller descending slope. This can be explained that, the axial capacity and the ability to resist deformation of concrete within spiral stirrup are improved under the dual constraints of both steel tube and spiral stirrup, as the damage process (volume expansion) of the concrete core is delayed. Overall, the parameter f_{yt} has little effect on the characteristics of the ascending branch of the $N-\Delta$ curve; however, the descending slope of the $N-\Delta$ curve after the peak load reduces with the increase of f_{yt} due to its increased restraint on the concrete core. Moreover, under the same parameters, square specimens generally possess a quicker load decrease after the peak load and a smaller Δ_{ue} than circular ones, considering that square tube has a weaker confinement to the concrete core than circular one [1]. It can also be observed from the measured $N-\Delta$ curves that, in general, the larger the volumetric stirrup ratio (ρ) of the specimens, the earlier the fracture of the spiral stirrup takes place in the post-peak stage, considering that the axial tensile stress of the stirrup under the same displacement increases with the increase of ρ; however, the relationship of the stirrup fracture moment with f_{yt} is not clear in this study.

The influence of parameters on load (N) versus strain (ε) relationship of the specimens is indicated in Fig. 8 by the solid lines, in which, the strains are the average values of those obtained in symmetrical measuring points. It is shown that, the overall characteristics of the $N-\varepsilon$ curves is similar to that of the $N-\Delta$ curves, that is, the $N-\varepsilon$ curves also contain three phases, i.e. elastic, elastic-plastic and post-peak. At the same time, the effect of ρ and f_{yt} on the $N-\varepsilon$ curves is also analogue to the $N-\Delta$ curves, i.e. the higher ρ and f_{yt} causes the larger initial slope and strain corresponding to the peak load and the slower the carrying capacity decreases in the post-peak stage. For square specimens, in general, there is little difference between the strains at sectional middle and those at sectional corner before the local buckling of the steel tube. After the local buckling of the steel tube, the strains at sectional corner are gradually greater than those at sectional middle, and the difference between them increases rapidly as the displacement increases until the end of the tests. This is mainly due to the fact that, the tube wall in the middle of the section gradually loses its bearing capacity after local buckling, so that the loads are transferred to the corner of the section. Furthermore, under the same parameters, the strain development of circular specimens is more sufficient than that of square specimens due to a better confinement of circular steel tube to the concrete core.

The relationship between strain ratio ($\varepsilon_{\mathrm{T}}/\varepsilon_{\mathrm{L}}$) and load level ($N/N_{\mathrm{ue}}$) of the specimens is displayed in Fig. 9, where ε_{T} and ε_{L} are the measured average transverse and longitudinal strain respectively, μ_{s} is the Poisson's ratio of the steel tube, and the capital letters 'M' and 'C' in Figs. 9(c) and (d) represent the sectional middle and corner of square specimens, respectively. It can be observed that, before reaching N_{ue} the $N/N_{\mathrm{ue}}-\varepsilon_{\mathrm{T}}/\varepsilon_{\mathrm{L}}$ relationship have certain variation trend; however, after reaching N_{ue} the $N/N_{\mathrm{ue}}-\varepsilon_{\mathrm{T}}/\varepsilon_{\mathrm{L}}$ relationship have no definite variation trend owing to the difference between the strain measuring points and the buckling position of the steel tube. Generally, with the first increase and then decrease of N/N_{ue}, the strain ratios ($\varepsilon_{\mathrm{T}}/\varepsilon_{\mathrm{L}}$) experience two stages of approaching and exceeding μ_{s}, respectively. During the former stage, the steel tube and concrete resist the loads more or less independently, and during the latter stage there is an obvious interaction between the steel tube and concrete core with the increased damage of concrete. At the same time, the two-stage boundary of circular specimens is at a N/N_{ue} of about 0.7, while the boundary of square specimen is at a N/N_{ue} of about 0.9, indicating that the interaction between the steel tube and concrete core of circular specimens occurs earlier than that of square ones. In addition, the difference in the $N/N_{\mathrm{ue}}-\varepsilon_{\mathrm{T}}/\varepsilon_{\mathrm{L}}$ relationship between sectional middle and corner of square specimens is not obvious. In general, the second stage of the $N/N_{\mathrm{ue}}-\varepsilon_{\mathrm{T}}/\varepsilon_{\mathrm{L}}$ relationship of specimens with spiral stirrup takes place later than that of specimens without spiral stirrup, and the higher the volumetric stirrup ratio (ρ) is, the later the second stage happens, mainly because the spiral stirrup constraint delays the damage process of the concrete core; however, the parameter f_{yt} has a moderate impact on the $N/N_{\mathrm{ue}}-\varepsilon_{\mathrm{T}}/\varepsilon_{\mathrm{L}}$ relationship of the specimens.

2.4.3. Mechanical indicators

The variation in the capacity (N_{ue}) and capacity improvement factor (F_{CI}) of the specimens is demonstrated in Fig. 10, and F_{CI} is defined as:

$$F_{\mathrm{CI}}=\frac{N_{\mathrm{ue,w}}-N_{\mathrm{ue,wo}}}{N_{\mathrm{ue,wo}}} \tag{4}$$

where, $N_{\mathrm{ue,w}}$ and $N_{\mathrm{ue,wo}}$ are the capacity of the specimens with spiral stirrup and the specimen without spiral stirrup, respectively.

It can be seen from Fig. 10 that, under the same condition of cross-section and f_{yt}, N_{ue} and F_{CI} of the specimens with spiral stirrup are higher than those of the reference specimen without spiral stirrup due to the enhanced constraint of the spiral stirrup to the concrete core. Meanwhile, the specimens with larger ρ and f_{yt} possess higher N_{ue} and F_{CI} owing to the increased dual confinement to the concrete core from both the steel tube and spiral stirrup. Moreover, under the same ρ and f_{yt}, square specimens result in larger N_{ue} and F_{CI} than circular ones, considering that, within the range of experimental parameters in this study, the increase of N_{ue} caused by the increased square specimen area is higher than that caused by the stronger confinement of circular steel tube to the concrete core, and in the case of the same cross-sectional area of the concrete confined by the stirrup, the spacing of spiral stirrup in the square specimens is smaller (see Table 1), that is, the spiral stirrup of square specimens provides a stronger constraint to the concrete inside. The calculating results indicate that, when $f_{yt} = 571.2$ MPa, N_{ue} of spiral stirrup reinforced circular (square) specimens with ρ of 0.7%, 1.2% and 2.4% is 1.1% (12.8%), 11.1% (10.1%) and 11.8% (22.0%) higher than the corresponding specimen without spiral stirrup respectively, and when $f_{yt} = 649.8$ MPa the percentage of improvement is 4.0% (21.6%), 11.5% (10.1%) and 23.3% (31.3%), respectively. It should be noticed that, N_{ue} and F_{CI} of square specimens having ρ=1.2% is abnormally high, which may be induced by the specimen fabrication deviation and/or the dispersion of material properties.

Refer to the method in [18], the composite elastic modulus (E_{sc}) of the specimens is defined as:

$$E_{sc} = \frac{0.4N_{ue}}{A_{sc} \cdot \varepsilon_{L,40\%}} \quad (5)$$

where, A_{sc} is overall cross-sectional area of the specimens, and $\varepsilon_{L,40\%}$ is average longitudinal strain corresponding to 40 percent of N_{ue} during the load rising phase.

Fig. 11 shows the variation in the composite elastic modulus (E_{sc}) of the specimens. It can be seen that, generally, E_{sc} of the spiral stirrup reinforced specimens is larger than that of the reference specimen without spiral stirrup, and the higher the volumetric stirrup ratio (ρ), the larger the composite elastic modulus (E_{sc}) is, especially for circular specimens. Meanwhile, except for two pairs of circular specimens with ρ of 1.2% and 2.4%, the specimens with a higher f_{yt} have a larger E_{sc}. This can be explained that, the concrete damage process becomes slower for the specimens with higher ρ and f_{yt}, i.e. the concrete has better resistance to volume increase after the destruction starts due to higher dual constraints of both the steel tube and spiral stirrup. In addition, compared with the specimens without spiral stirrup, the ratio of E_{sc} improvement of the spiral stirrup reinforced circular specimens is higher than that of the spiral stirrup reinforced square specimens. Further calculation results show that, with f_{yt} of 571.2 MPa, the circular (square) specimens with ρ of 0.7%, 1.2% and 2.4% respectively result in 15.3% (0.0%), 32.1% (1.8%) and 38.1% (6.5%) higher E_{sc} than the reference specimen with ρ=0, and with f_{yt} of 649.8 MPa the corresponding percentage of improvement is 8.8% (0.0%), 19.0% (0.2%) and 21.2% (18.5%), respectively.

Similar to the relevant studies [18], the ductility coefficient (μ) of the specimens with and without spiral stirrup can be determined by the following equation:

$$\mu = \frac{\Delta_{ap,85\%}}{\Delta_{ue}} \quad (6)$$

where, $\Delta_{ap,85\%}$ is the displacement in the post-peak stage when the load drops to 85 percent of N_{ue}.

Fig. 12 indicates the effect of parameters on μ of the specimens. It can be found that, generally, μ increases with the increase of ρ and f_{yt}, and circular specimens possess a larger μ than square ones under the same deminsionless parameters. This is also due to the fact that, the dual constraints of the steel tube and spiral stirrup to the concrete core increases with the increase of ρ and f_{yt}, and circular steel tube provides a better constraint to concrete core than square steel tube. Overall, while f_{yt}=571.2 MPa, μ of circular (square) specimens having ρ of 0.7%, 1.2% and 2.4% is 1.11 (1.10), 1.16 (1.20) and 1.36 (1.32) times that of the reference unreinforced specimen (ρ=0), and while f_{yt}=649.8 MPa the corresponding ratios are 1.28 (1.17), 1.58 (1.28) and 1.72 (1.44), respectively.

3. Finite element (FE) simulation

3.1. Description of the FE model

The widely used software ABAQUS [19] was employed to establish the finite element (FE) model of axially compressed CTHST stub columns with inner spiral stirrup.

The 4-node reduced-integration shell elements (S4R) having 9 integration points and the linear truss elements (T3D2) were used to simulate the steel tube and the spiral stirrup, respectively. To avoid shear self-locking, the reduced-integration brick elements with 8 nodes (C3D8R) were used to simulate the concrete core and the whole steel sleeves (including endplate and stiffeners). Contacts between different components were further defined to closely reproduce actual loading process of axially compressed CTHST stub columns with inner spiral stirrup. For the contact between the concrete and steel tube, the tube inner wall and the concrete surface in contact with the tube inner wall were respectively defined as master and slave surface, and the hard contact and the Coulomb friction model were chosen to replicate the interaction in the normal and tangential directions of the contact surface, respectively. Meanwhile, a friction coefficient of 0.6 in the tangential directions was selected for the Coulomb friction model. The contact between concrete and endplate on the steel sleeve was the same as that between concrete and steel tube, and the contact between the spiral stirrup and concrete was reproduced by the 'Embedded' constraint. Moreover, the 'Tie' constraint was used between the steel tube and the sleeve (including the endplate), and the sleeve together with the endplate and stiffeners on it were taken as a whole with the 'Tie' constraint.

In the FE modelling, the material of the steel tube and spiral stirrup were simulated by the elastic-plastic model. The five-segment model in [20] was selected to describe the engineering stress (σ_s)−strain (ε_s) relationship of circular steel tube. The four-segment model in [21] was used to obtain the engineering $\sigma_s - \varepsilon_s$ relationship of flat and corner parts in the cold-formed square steel tube, and the corner radius of the cold-formed square steel tube was determined according to the method provided by Elchalakani et al. [22]. Moreover, in the FE simulation, the measured elastic modulus and Poisson's ratio of the steel tube (see Table 2) were used, and the sleeves (including the endplate) were simulated as a kind of pure elastic material with elastic modulus and Poisson's ratio of 1.0×10^8 N/mm^2 and 0.001, respectively.

For the spiral stirrup, the well-known bilinear engineering $\sigma_s - \varepsilon_s$ relationship was employed to capture the failure process of the spiral stirrup from crack initiation (i.e. reaching the ultimate strain) to complete fracture. It is assumed that the engineering stress decreases linearly with the increase of engineering strain until it equals to zero while fracture strain reached. The detailed engineering $\sigma_s - \varepsilon_s$ relationship of spiral stirrup is as follows:

$$\sigma_s = \begin{cases} E_s \cdot \varepsilon_s & (\varepsilon_s < \varepsilon_y) \\ f_{ys} + \frac{(f_{us} - f_{ys})}{(\varepsilon_u - \varepsilon_y)} \cdot (\varepsilon_s - \varepsilon_y) & (\varepsilon_y \le \varepsilon_s < \varepsilon_u) \\ f_{us} - 0.34 E_s \cdot (\varepsilon_s - \varepsilon_u) & (\varepsilon_u \le \varepsilon_s < \varepsilon_f) \\ 0 & (\varepsilon_s > \varepsilon_f) \end{cases} \tag{7}$$

where, $\varepsilon_y (= f_{ys}/E_s)$ is the yield strain; f_{us} is the tensile strength; ε_u is the ultimate strain, which equals to the measured value or 4.5% (when there is no measured value), ε_f is the fracture strain (i.e. elongation ratio), which equals to the measured value or 5.0% (while no measured value available). In the actual simulation, to avoid the non-convergence caused by the fracture of spiral stirrup, the engineering stress was set to be a very small value when ε_f was attained.

The concrete was simulated by the damage plasticity model in ABAQUS [19]. The uniaxial compressive stress (σ_c)−strain (ε_c) model presented by Han et al. [23] was used to obtain stress versus non-elastic strain relationship of the concrete core, and the detailed formulae for the $\sigma_c - \varepsilon_c$ relationship are as follows:

$$y = \begin{cases} 2x - x^2 & (x \le 1) \\ x/[\omega \cdot (x-1)^\eta + x] & (x > 1) \end{cases} \tag{8}$$

where, $y = \sigma_c / f_c'$; $x = \varepsilon_c / \varepsilon_0$; $\varepsilon_0 = (1300 + 12.5 f_c' + 800 \xi^{0.2})/1\mathrm{E}6$; for circular section, $\omega = 0.5(f_c')^{0.5} \cdot (2.36\mathrm{E}-5)^{[0.25+(\xi-0.5)^7]}$ and $\eta = 2.0$, and for square section, $\omega = (f_c')^{0.1}/[1.2(1+\xi)^{0.5}]$ and $\eta = 1.6 + 1.5/x$; f_c' is the cylindrical compressive strength of concrete; and ξ $(=\alpha_n \cdot f_{yt}/f_{ck})$ is the confinement factor [23], in which f_{ck} is the characteristic compressive strength of concrete.

The concrete tension stiffening was modelled by the relationship between tensile stress and cracking energy [19], and the peak stress was equal to $0.1 f_c'$. Furthermore, the equation in [24] was used to obtain E_c and Poisson's ratio of concrete was equal to 0.2.

Full model was built to carry out the FE simulation on the behaviour of axially compressed CTHST stub columns with inner spiral stirrup, and the mesh division and boundary conditions used are shown in Fig. 13. All translational and rotational degrees of freedom of bottom surface of the model are restricted (i.e. 'ENCASTRE' in ABAQUS [19]) to reappear the reaction of the lower platen of the tester, and the translational degrees of freedom in the X and Y directions of top surface of the model are restricted to reproduce the upper spherical hinge of the tester. During the simulation, displacement-controlled loading was used, and a displacement of 40 mm along the Z direction was applied to the top surface of the model.

3.2. Validation of the FE model

Fig. 14 shows the simulated failure pattern of the steel tube, concrete core and spiral stirrup with initial fracture of typical specimens, where the steel tube and spiral stirrup are presented with the Mises stresses and the concrete core is presented with the logarithmic strain (LE33). From the comparison between the simulated failure pattern of the steel tube and concrete core in Fig. 14 and the experimental results in Figs. 5 and 6, it can be observed that, for circular specimens without spiral stirrup, outward bulging of the steel tube near half-height area due to the expansion of concrete core is obtained by the FE simulation; however, for circular specimens with spiral stirrup, the simulated failure patterns are demonstrated as the local buckling of the steel tube and failure of concrete core (i.e. the area with higher LE33) within several spacings of spiral stirrup. These are different from the observations in Figs. 5 and 6, and the reason is that the complex loading process of the specimens in the late stage of the tests, such as random failure locations caused by the randomness of material defects distribution, eccentric loading caused by asymmetry failure, is difficult to realize in the FE simulation. For square specimens, the simulated deformation shape and quantity of outward buckling of the steel tube, together with failure of concrete near the buckling positions of the steel tube, are generally consistent with the experimental observations, but the buckling positions of the steel tube are different from the experimental phenomenon to some extent. In addition, the predicted results in Fig. 14(c) show that, in general, the initial fracture of spiral stirrup (marked by an arrow) in the specimens happens near the half-height section.

The contrast between the simulated and recorded load (N) versus deformation (Δ or ε) relationship is demonstrated in Figs. 7, 8 and 15, where the experimental results in this study and the literature [6][10] are also included. It is shown that, in general, the simulated trend of load as the deformation increases is in good agreement with the measured results. However, the simulated initial slope of $N-\Delta$ curve of the specimens in this study is significantly steeper than the measured results. It may be due to the fact that, the possible factors leading to the reduction of the axial compression stiffness of the specimens, such as the imperfection and/or defect of the specimens and the testing process, the deviation of the actual sizes from the design sizes and the small initial eccentricity of the loads, cannot be reasonably reflected in the FE model. Moreover, there is also a certain difference between the post-peak stage of the simulated $N-\Delta(\varepsilon)$ curves and the measured results, mainly because there may be a lower estimation of the modulus of the steel tube and/or spiral stirrup after yielding, and the bulging positions of the steel tube in the specimens are not completely located at the positions having the strain gauges.

Fig. 16 displays the comparison between the predicted and measured mechanical indicators. The results show that, for the specimens in this study, the mean and standard deviation of $N_{\mathrm{u,fe}}/N_{\mathrm{u,e}}$ ($E_{\mathrm{sc,fe}}/E_{\mathrm{sc,e}}$) equal to 0.960 (1.039) and 0.041 (0.096), respectively, and the difference between the predicted and measured results is generally within 15%. In addition, for the specimens in the literature [6][10], the value of $N_{\mathrm{u,fe}}/N_{\mathrm{u,e}}$ has the mean and standard deviation of 0.986 and 0.033 with the maximum and minimum of 1.026 and 0.921. These comparison results mean that the constructed FE model has the ability of well predicting the capacity and composite elastic modulus of axially compressed CTHST stub columns with inner spiral stirrup.

3.3. Mechanism analysis using the FE model

The FE model is further used to carry out the mechanism analysis of typical CTHST stub columns with inner spiral stirrup while the volumetric stirrup ratio (ρ) changes, and the fundamental information of calculating examples includes: D=400 mm, α_{n}=0.12, f_{yt}=460 MPa, f_{ys}=500 MPa, and f_c'=50 MPa.

Fig. 17 shows the load (N) versus longitudinal strain (ε_L) curve of typical composite members, where the arrow positions are also the moment when the fracture of spiral stirrup occurs. It can be observed that, the simulated $N-\varepsilon_L$ curves are generally similar to the measured results in this study (see Fig. 8), i.e. the curve consists of three variation stages with sudden drop in load carrying capacity after the initial fracture of spiral stirrup, and with the increase of ρ the capacity (N_u) increases, the load drop rate in the post-peak stage decreases, and the longitudinal strain corresponding to fracture of spiral stirrup increases. Moreover, under the same parametric conditions, circular column has a slower load drop rate in the post-peak stage and a later initial fracture of spiral stirrup than square one. When the longitudinal strain reaches 0.02, there is no fracture of spiral stirrup in circular members; however, the fracture of spiral stirrup in square members may take place. To facilitate the analysis, three key points on the $N-\varepsilon_L$ curves are selected to reveal the representative mechanism of such composite members, where points A, B and C corresponds to N of $0.4N_u$, N of N_u and ε_L of 0.02, respectively.

The simulated results show that, the volumetric stirrup ratio (ρ) has little influence on the stress state of the steel tube, but has a more obvious effect on the stress state of the concrete core and spiral stirrup of axially compressed CTHST stub columns with inner spiral stirrup, as indicated in Fig. 18, where the longitudinal stress of concrete (S33) is taken from the half-height section. It can be seen from Fig. 18(a) that, at point A, the S33 of circular column with spiral stirrup exhibiting a characteristic of decrease from center to perimeter is different from that of circular column without spiral stirrup having a characteristic of increase from center to perimeter (stress gradient is very small), whilst, the S33 of square column with spiral stirrup forming an evident high stress central area is also different from that of square column without spiral stirrup having an even distribution. This can be explained that, the presence of spiral stirrup makes the concrete inside the stirrup confined from the start of loading, and thus affects the stress state of concrete core. At points B and C, the effect of ρ on the distribution characteristics of S33 is not obvious since the Mises stress of the stirrup has reached the yield strength (see Fig. 18(b)), that is, the S33 of circular column is evenly distributed along the circumference and exhibits a characteristic of decrease from center to perimeter, and the S33 of square column is the largest at the corner and forms a high stress area in which the corner is connected to the core, while decays from the corner/center to the middle of the four sides. Moreover, the S33 of concrete core increases with the increase of ρ owing to the increased confinement from the spiral stirrup. The results in Fig. 18(b) demonstrate that, the high stress area of the spiral stirrup appears in the middle of column height. The Mises stress of the spiral stirrup at point A is about 15% of its yield strength, and at point B, the Mises stress of the spiral stirrup in the middle of column height has exceeded its yield strength. At point C, the Mises stress of the spiral stirrup continues to increase, and the spiral stirrup of circular column are not broken while the spiral stirrup near the half-height section of square column is broken. In general, the volumetric stirrup ratio (ρ) has little effect on the Mises stress distribution of the spiral stirrup.

Fig. 19 shows the effect of ρ on the interaction stresses between the steel tube and concrete core (q) within one spacing of the spiral stirrup (s) at the half-height section, where z is the distance from the half-height section. The results indicate that, consistent with square CFST columns, q at the sectional middle of square CTHST columns is close to zero, thus only the change of q at the sectional corner of square composite columns is analyzed. It can be seen from Fig. 19 (a) that, q of circular column without spiral stirrup are almost uniformly distributed; however, q of circular column with spiral stirrup are the largest at half-spacing site and decreases from the half-spacing site to the location of the stirrup due to the constraint effect of the stirrup to the concrete core [25]. Generally, at point A, q of circular column with spiral stirrup is higher than that of circular column without spiral stirrup, whilst, at points B and C, q of circular column with spiral stirrup is lower than that of circular column without spiral stirrup, as the unbroken stirrups can well limit the volume expansion of concrete, thus reducing the interaction between steel tube and concrete core. Moreover, with the change of ρ, q of circular column displays different change rules at three points, which is mainly due to the determination of ρ on the stress state of the steel tube and concrete. The data in

Fig. 19(b) demonstrate that, regardless of spiral stirrup, q reaches its maximum at point B, and the q at points A and C is much lower than that at point B. For square column without spiral stirrup, q at points A and B are almost uniformly distributed; however, q at point C presents the characteristics of low at buckling position and high at non-buckling position of the steel tube, considering that local buckling happens at the half-height section of the steel tube. Simutaneously, for square column with spiral stirrup, q at point B is almost uniformly distributed; however, q at points A and C presents the characteristics similar to that at point C of square column withou spiral stirrup. Furthermore, q at three points of square column decreases with the increase of ρ, as the restriction effect of spiral stirrup on concrete expansion is enhanced.

4. Calculation method for the capacity

It is well known that, the load carrying capacity of the concrete confined by stirrups will be improved [25], which should be taken into account when calculating the capacity of CTHST members with inner spiral stirrup. The proposed equations for the peak compressive stress of stirrup-confined concrete (f_{cc}) in [26], which are obtained by regression on a large number of experimental data and have the best calculation results compared with other existing methods, are selected to calculate the compressive strength of the confined concrete in the CTHST stub columns with inner spiral stirrup, and the detailed equations are as follows:

$$\frac{f_{cc}}{f_c'} = 1 + 5.35 f_l^{-0.14} \cdot \frac{f_l}{f_c'} \tag{9}$$

$$f_l = \frac{2 f_{ys} \cdot A_{s,s}}{D_s \cdot s} \tag{10}$$

where, f_l is the lateral pressure on the concrete.

Fig. 20 is a schematic diagram of the concrete compressive strength distribution in the CTHST cross-section with the confinement effect of spiral stirrup introduced while reaching the capacity. It is shown that, the core concrete of a circular section can be treated as one area with uniform compressive strength of f_{cc}, and meanwhile the core concrete of a square section can be divided into two areas with the compressive strength of f_{cc} and f_c', respectively. Based on the above distribution characteristics, a CTHST stub column with inner spiral stirrup is transformed into a circular CTHST stub column with the same concrete compressive strength or a square CTHST stub column with different concrete compressive strengths. Through the investigation and judgment of the existing calculation methods, it is found that the formulae in [27] can be well applied to the capacity calculation of CTHST stub columns with the concrete compressive strength distribution characteristics shown in Fig. 20 by appropriate adjustments. The final formulae for the capacity of CTHST stub columns with inner spiral stirrup are as follows:

$$N_{\mathrm{u}}=\begin{cases}\eta_{\mathrm{ao}}\cdot f_{\mathrm{yt}}\cdot A_{\mathrm{s}}+A_{\mathrm{c}}\cdot f_{\mathrm{cc}}\cdot\left(1+\eta_{\mathrm{co}}\cdot\frac{t}{D}\cdot\frac{f_{\mathrm{yt}}}{f_{\mathrm{cc}}}\right) & \text{Circular section}\\ f_{\mathrm{yt}}\cdot A_{\mathrm{s}}+A_{\mathrm{c1}}\cdot f_{\mathrm{cc}}+A_{\mathrm{c2}}\cdot f_{\mathrm{c}}' & \text{Square section}\end{cases}\tag{11}$$

where, η_{ao} and η_{co} are the coefficient related to the relative slenderness [27], and A_{c1} and A_{c2} are the concrete area of square section with and without stirrup confinement, respectively.

Fig 21 shows the comparison between the calculated capacities ($N_{\mathrm{u,s}}$) of axially compressed CTHST specimens with inner spiral stirrup using Eq. (11) and the experimental results ($N_{\mathrm{u,e}}$) in the literature [6][10] and this study. The statistical analysis on the results in Fig. 21 shows that, the mean and standard deviation of $N_{\mathrm{u,s}}/N_{\mathrm{u,e}}$ are 1.035 and 0.046 respectively, and the overall difference between the simplified and measured results is within 10%. The comparison results show that, Eq. (11) can be practically applied for the capacity prediction of axially compressed CTHST stub columns with inner spiral stirrup. According to the experiments as well as numerical simulation in the literature and this paper, the application range of Eq. (11) is: D=220-400 mm, α_{n}=0.05-0.15, $\rho \leq 2.4\%$, f_{yt}=324.3-648.9 MPa, f_{ys}=363.5-1074.1 MPa, and f_{c}'=32.1-79.6 MPa.

5. Conclusions

The experimental and numerical studies on the behaviour of axially compressed concrete-filled thin-walled high-strength steel tube (CTHST) stub columns with inner spiral stirrup are carried out, and within the range of parameters considered in this study the main conclusions are as follows:

(1) In general, irrespective of inner spiral stirrup, shear failure along diagonal plane of both tube and concrete core and local buckling of tube together with crushing of concrete at the location of wall

buckling are the main failure characteristics of circular and square specimens, respectively. Simultaneously, the volumetric stirrup ratio (ρ) affects the horizontal angle of failure plane of the specimens and the buckling level at the corner of square specimens; however, the yield strength of steel tube (f_{yt}) has a moderate effect on the failure pattern of the specimens. Furthermore, the fracture of inner spiral stirrup of the specimens occurred at least once.

(2) Specimens with larger ρ and f_{yt} show a higher initial slope, a longer elastic-plastic phase, a larger deformation corresponding to peak load and a slower load decrease in the post-peak phase of load (N) versus displacement/strain (Δ/ε) curves. Moreover, the load drop in the post-peak phase of square specimens is more abruptly than that of circular specimens due to weaker confinement of square steel tube to the concrete core.

(3) The capacity (N_{ue}), composite elastic modulus (E_{sc}) and ductility coefficient (μ) of specimens with inner spiral stirrup are higher than those of specimens without inner spiral stirrup, and the larger ρ and f_{yt} of the specimens, the larger the mechanical indicators (N_{ue}, E_{sc} and μ) are. In addition, under the same conditions, circular specimens with inner spiral stirrup result in a higher improvement of N_{ue} and E_{sc} and a larger μ than the corresponding square specimens with inner spiral stirrup.

(4) The finite element (FE) model can well simulate the behaviour of axially compressed CTHST stub columns with inner spiral stirrup. Further FE simulation results show that, ρ mainly affects the stress state of concrete and stirrup during the loading process. Moreover, due to the constraint effect of spiral stirrup, the interaction stress between steel tube and concrete core (q) of CTHST columns with spiral stirrup presents different distribution characteristics from that of CTHST columns without spiral stirrup.

(5) With the consideration of concrete strength in different regions across the cross-section , the formulae for calculating the capacity of CTHST stub columns with inner spiral stirrup is proposed by properly revising the equations in EN 1994-1-1, and the simplified calculation results are generally in good agreement with the experimental results.

It is evident that most columns in practice are much longer than the tested specimens (stub columns) in this paper, and the failure pattern, load versus deformation relationship and bearing capacity of the long/slender composite columns are significantly different from the stub ones under the effect of slenderness ratio. The experimental observations, numerical method and simplified formulae in this study can provide a basis for further study on the performance and design method of the long/slender CTHST columns with inner spiral stirrup.

Declaration of Competing Interest

The authors declare that they have no known competing financial interests or personal relationships that could have appeared to influence the work reported in this paper.

Acknowledgement:

The research work reported herein was supported by the National Natural Science Foundation of China (No. 51678105). The research funding is highly appreciated. The authors also wish to thank Ms. Min Hou for her help in the tests.

References:

[1] Han LH, Li W, Bjorhovde R. Developments and advanced applications of concrete-filled steel tubular (CFST) structures: Members. J. Constr. Steel Res. 2014;100:211-228.

[2] Han LH, Yang YF, Yang H, Li W. Life-cycle based analytical theory of concrete-filled steel tubular structures and its applications. Chin. Sci. Bull. 2020;65(28-29):3173-3184. (in Chinese)

[3] Zhong Y, Sun Y, Tan KH, Zhao O. Testing, modelling and design of high strength concrete-filled high strength steel tube (HCFHST) stub columns under combined compression and bending. Eng. Struct. 2021;241:112334.

[4] Lie TT. Fire resistance of circular steel columns filled with bar-reinforced concrete. J. Struct. Eng. ASCE 1994;120(5):1489-1509.

[5] Lie TT, Kodur VKR. Fire resistance of steel columns filled with bar-reinforced concrete. J. Struct. Eng. ASCE 1996;122(1):30-36.

[6] Ding F, Fang C, Bai Y, Gong Y. Mechanical performance of stirrup-confined concrete-filled steel tubular stub columns under axial loading. J. Constr. Steel Res. 2014;98:146-157.

[7] Lai MH, Ho JCM. Effect of continuous spirals on uni-axial strength and ductility of CFST columns. J. Constr. Steel Res. 2015:104:235-249.

[8] Hu HS, Xu L, Guo ZX, Shahrooz BM. Behavior of eccentrically loaded square spiral-confined high-strength concrete-filled steel tube columns. Eng. Struct. 2020;216:110743.

[9] Xiamuxi A, Liu X, Hasegawa A. Study of the concrete in reinforced concrete-filled steel tube column under axial loading. J. Constr. Steel Res. 2020;170:106111.

[10] Teng JG, Wang JJ, Lin G, Zhang J, Feng P. Compressive behavior of concrete-filled steel tubular columns with internal high-strength steel spiral confinement. Adv. Struct. Eng. 2021;24(8):1687-1708.

[11] Chen Z, Zhou J, Jing C, Tan Q. Mechanical behavior of spiral stirrup reinforced concrete filled square steel tubular columns under compression. Eng. Struct. 2021;226:111377.

[12] Farmani MA, Heidarpour A, Zhao XL. A distinctive approach to testing and modeling thermal creep in ultra-high strength steel. Int. J. Mech. Sci. 2021;198:106362.

[13] Sun M, Du C, Liu Z, Liu C, Li X, Wu Y. Fundamental understanding on the effect of Cr on corrosion resistance of weathering steel in simulated tropical marine atmosphere. Corros. Sci. 2021:186:109427.

[14] Abbas S, Nehdi ML, Saleem MA. Ultra-high performance concrete: mechanical performance, durability, sustainability and implementation challenges. Int. J. Concr. Struct. M. 2016;10(3): 271-295.

[15] Xiong MX, Xiong DX, Liew JYR. Axial performance of short concrete filled steel tubes with high- and ultra-high-strength materials. Eng. Struct. 2017;136:494-510.

[16] Du Y, Chen Z, Wang Y B, Liew JYR. Ultimate resistance behavior of rectangular concrete-filled tubular beam-columns made of high-strength steel. J. Constr. Steel Res. 2017;133:418-433.

[17] Wu H, Ren GM, Fang Q, Liu JZ. Response of ultra-high performance cementitious composites filled steel tube (UHPCC-FST) subjected to low-velocity impact. Thin-Walled Struct. 2019;144: 106341.

[18] Yang YF, Hou C, Liu M. Tests and numerical simulation of rectangular RACFST stub columns under concentric compression. Structures 2020;27:396-410.

[19] Simulia. ABAQUS analysis user's guide, version 6.14. Providence, RI: Dassault Systèmes Simulia Corp., 2014.

[20] Yang YF, Fu F, Bie XM, Dai XH. Axial compressive behaviour of CFDST stub columns with large void ratio. J. Constr. Steel Res. 2021;186:106892.

[21] Abdel-Rahman N, Sivakumaran KS. Material properties models for analysis of cold-formed steel members. J. Struct. Eng. ASCE 1997;123(9):1135-1143.

[22] Elchalakani M, Zhao XL, Grzebieta R. Tests on concrete filled double-skin (CHS outer and SHS inner) composite short columns under axial compression. Thin-Walled Struct. 2002;40(5):415-441.

[23] Han LH, Yao GH, Tao Z. Performance of concrete-filled thin-walled steel tubes under pure torsion. Thin-Walled Struct. 2007;45(1):24-36.

[24] ACI Committee 318. Building code requirements for structural concrete (ACI 318-19) and commentary. American Concrete Institute, Detroit, USA, 2019.

[25] Park R, Paulay T. Reinforced concrete structures. New York: John Wiley & Sons, 1975.

[26] Wei Y, Wu YF. Compression behavior of concrete columns confined by high strength steel wire. Constr. Build. Mater. 2014;54:443-453.

[27] CEN. EN 1994-1-1, Eurocode 4: Design of composite steel and concrete structures-Part 1-1: General rules and rules for buildings. European Committee for Standardization, Brussels, Belgium, 2004.

Replies to Reviewer's Comments

Structures

Manuscript: Behaviour of axially compressed CTHST stub columns with inner spiral stirrup (Ref. No.: STRUCTURES-D-22-02887)

Authors: You-Fu Yang*, Yu-Qin Zhang, Feng Fu
(* Corresponding author: youfuyang@163.com)

The authors wish to thank the reviewers' comments which certainly enhance the quality of the paper.

The authors have checked all the editorial revisions and the comments from the reviewers and revised the manuscripts accordingly. The changes we have made in response to the reviewers' comments are listed in the following tables.

Reviewer #1

Comment No.	Comments, replies and changes made.	
General Comment	Comment	This paper presents an investigation on the behaviour of axially compressed CTHST stub columns with inner spiral stirrup. A group of specimens was tested. The developed FE model was validated and accepted agreement achieved. Simple analysis/calculation method was developed to assess the ultimate strength of stub composite columns with inner stirrup. The subject matter is interesting and within the scope of the journal and the research content is original. The experimental data and simple calculation method and analysis may be reference for further numerical model validation, parameter study and design engineers' consideration. The paper is well written and organized. Suggested to improve/clarify the following points.
	Replies	The authors greatly appreciate the reviewer's recommendation and comments. Addressing the reviewers' comments has significantly improved the quality of this paper, which can be seen from the detailed changes summarized in this report.
Technical Comment 1	Comment	Please further clarify/discuss the effect of steel sleeves at both ends to the failure modes.
	Replies	The authors agree with the reviewer on that the effect of steel sleeves at both ends to the failure modes should be further discussed.
	Changes made	The following text has been added in page 7 of the revised manuscript: As can be seen in the pictures, there is no sign of damage within the range of specimen ends covered by the sleeve, showing that the sleeve can effectively prevent the destruction of the specimen ends, and thus the failure occurs near the half-height region of the specimen having more uniform properties.
Technical Comment	Comment	In practice, most columns will be much longer than the length of the tested specimens, how do you foresee the difference of the load capacity, failure

2		modes of long/slender composite columns? Will the research outcomes be valuable for similar slender composite column design?
	Replies	The authors agree with the reviewer's comment. The related foreseeing contents have been provided in the revised manuscript.
	Changes made	The following text has been added in page 22 of the revised manuscript: It is evident that most columns in practice are much longer than the tested specimens (stub columns) in this paper, and the failure pattern, load versus deformation relationship and bearing capacity of the long/slender composite columns are significantly different from the stub ones under the effect of slenderness ratio. The experimental observations, numerical method and simplified formulae in this study can provide a basis for further study on the performance and design method of the long/slender CTHST columns with inner spiral stirrup.
Technical Comment 3	Comment	Discuss/clarify the application range and limitation of your research results/conclusions due to the specimen limitation, such as section dimensions, length, material grades etc.
	Replies	The authors agree with the reviewer's comment.
	Changes made	The following text has been added in page 20 of the revised manuscript: According to the experiments as well as numerical simulation in the literature and this paper, the application range of Eq. (11) is: D=220-400 mm, α_n=0.05-0.15, $\rho \leq 2.4\%$, f_{yt}=324.3-648.9 MPa, f_{ys}=363.5-1074.1 MPa, and f_c'=32.1-79.6 MPa. … and within the range of parameters considered in this study the main conclusions are …

Reviewer #2

Comment No.	Comments, replies and changes made.	
General Comment	Comment	The authors investigated the behavior of CFHST columns reinforced with spiral stirrups. Interesting results were achieved concerning the effects of spiral on the load-bearing capacity and ductility of CFHST columns. The manuscript is well organized and the behavior of the composite columns is well investigated. This manuscript can be accepted with minor revisions. The reviewer provides the following comments for consideration:
	Replies	The authors greatly appreciate the reviewer's recommendation and comments. Addressing the reviewers' comments has significantly improved the quality of this paper, which can be seen from the detailed changes summarized in this report.
Technical Comment	Comment	Fig.6: It would be good if the fracture of the spiral can be more clearly presented and denoted, as spiral fracture is part of the failure mode of

1		specimens.
	Replies	The authors agree with the reviewer's comment. The concrete near the fracture position of the spiral stirrup should be removed to clearly show the failure pattern of the spiral stirrup. However, due to the negligence of the authors and the limit space of the lab, the damaged specimens were thrown away as waste by lab technicians after we completed the fracture location inspection of the spiral stirrup. We apologize for not being able to provide a clearer picture of the stirrup fracture.
	Changes made	There is no change in the revised manuscript.
Technical Comment 2	Comment	Fig. 7: It seems that the modelling results have a much steeper slope than the experimental results in the elastic stage. Why? Additionally, the residual loads in the descending stage of some circular specimens are lower than the experimental curves. Could this be due to a lower estimation of the modulus of steel tube or spiral after yielding?
	Replies	The authors agree with the reviewer's comment. The reason for the difference between the simulated and measured curves needs in-depth analysis.
	Changes made	The following text has been added in page 16 of the revised manuscript to explain the reason: However, the simulated initial slope of $N-\Delta$ curve of the specimens in this study is significantly steeper than the measured results. It may be due to the fact that, the possible factors leading to the reduction of the axial compression stiffness of the specimens, such as the imperfection and/or defect of the specimens and the testing process, the deviation of the actual sizes from the design sizes and the small initial eccentricity of the loads, cannot be reasonably reflected in the FE model. Moreover, there is also a certain difference between the post-peak stage of the simulated $N-\Delta(\varepsilon)$ curves and the measured results, mainly because there may be a lower estimation of the modulus of the steel tube and/or spiral stirrup after yielding, and the bulging positions of the steel tube in the specimens are not completely located at the positions having the strain gauges.
Technical Comment 3	Comment	L345 Should fyt be substituted with fys?
	Replies	The authors agree with the reviewer's comment.
	Changes made	The variable fyt has been substituted with fys in the revised manuscript: $$\sigma_s = \begin{cases} E_s \cdot \varepsilon_s & (\varepsilon_s < \varepsilon_y) \\ f_{ys} + \frac{(f_{us} - f_{ys})}{(\varepsilon_u - \varepsilon_y)} \cdot (\varepsilon_s - \varepsilon_y) & (\varepsilon_y \le \varepsilon_s < \varepsilon_u) \\ f_{us} - 0.34 E_s \cdot (\varepsilon_s - \varepsilon_u) & (\varepsilon_u \le \varepsilon_s < \varepsilon_f) \\ 0 & (\varepsilon_s > \varepsilon_f) \end{cases} \quad (7)$$
Technical Comment	Comment	L358 It would be good if an explanation for αn can be provided.
	Replies	Explanation for αn is in lines 113 and 114 of the original manuscript. Now,

4		the explanation for αn is in lines 4 and 5 on page 5 of the revised manuscript.
	Changes made	The explanation for αn is as follows: …, where α_n is the nominal cross-sectional steel ratio equal to the ratio of the area of the steel tube to that enclosed by the tube inner wall, …
Technical Comment 5	Comment	Section 3.1 and Fig.14: According to Fig. 14, the failure mode was not symmetric to the mid-height plane. How is this achieved through FE modelling?
	Replies	On the one hand, we did not take special settings in the FE modelling to obtain simulation results more consistent with the test results, that is, without considering the spiral stirrup, the loading, boundary conditions and meshing of all FE models are symmetric, as shown in Fig. 13. On the other hand, we believe that the main reason for the asymmetry of the failure pattern with respect to the mid-height plane is the existence of the spiral stirrup, which is asymmetric with respect to the mid-height plane.
	Changes made	There is no change in the revised manuscript.
Technical Comment 6	Comment	L 369: The authors stated that a displacement of 40 mm was applied, which led to an axial strain of 40/720=0.056. However, the strain in concrete (LE33) in Fig. 14 seems to have exceeded 0.1, and the legend is not clear enough. Please check the data and substitute the legends with clearer ones.
	Replies	The displacement of 40 mm is correct and the strains in concrete (LE33) are also the corresponding results. The reason is as follows: If the axial strain is calculated according to 40/720=0.056, it is equivalent to the default that the column is uniformly deformed along axial direction, that is, the axial strain at each position along the height direction is the same. However, the simulation results in Fig. 14 show that, the column axial deformation (strain) are mainly concentrated in the half-height of a certain area (i.e. steel tube buckling range), and the axial strain of the rest part of the column is very small. As a result, the actual height with main deformation (e.g. axial strain) is far less than 720 mm, producing a local axial strain greater than 0.056 in the half-height area, and the longitudinal strain is much larger at the position having maximum local buckling of the steel tube. The legends in Fig. 14 are indeed not clear enough.
	Changes made	The figures with clear legends have been added to the revised manuscript.
Technical Comment 7	Comment	There are some grammatical errors in this manuscript. Additionally, some sentences should be rephrased to improve quality of this manuscript. The following are only some examples: L94: There should be an "and" before "no research". L97-99: "The objective of the paper is thus to experimentally assess the axial compressive performance of CTHST stub columns with inner spiral stirrup." Since FE modelling was also conducted, it may be inappropriate to use "experimentally" here.

		L99-100: "Tests of 16 specimens were carried out to evaluate the effect of two variables…". The two variables can be substituted with "volumetric ratio of stirrup and yield strength of steel tube". L15 and L513: There are both "volumetric stirrup ratio" and "volume stirrup ratio" in this manuscript. Please use a consistent expression. L520: "faster"---"more abruptly" L532: What do the authors mean by "numerical changes"
	Replies	The authors agree with the reviewer's comment.
	Changes made	The above grammatical errors have been corrected in the revised manuscript. L94: … premature, and no L97-99: The objective of the paper is thus to experimentally and numerically assess the axial compressive performance of CTHST stub columns with inner spiral stirrup. L99-100: Tests of 16 specimens were carried out to evaluate the effect of volumetric stirrup ratio and yield strength of steel tube on the failure L15 and L513: 'volumetric stirrup ratio' is used. L529: … specimens is more abruptly than that … L541: the words of "numerical changes" are deleted. By the way, the revised manuscript was also thoroughly checked to avoid errors.

Figures:

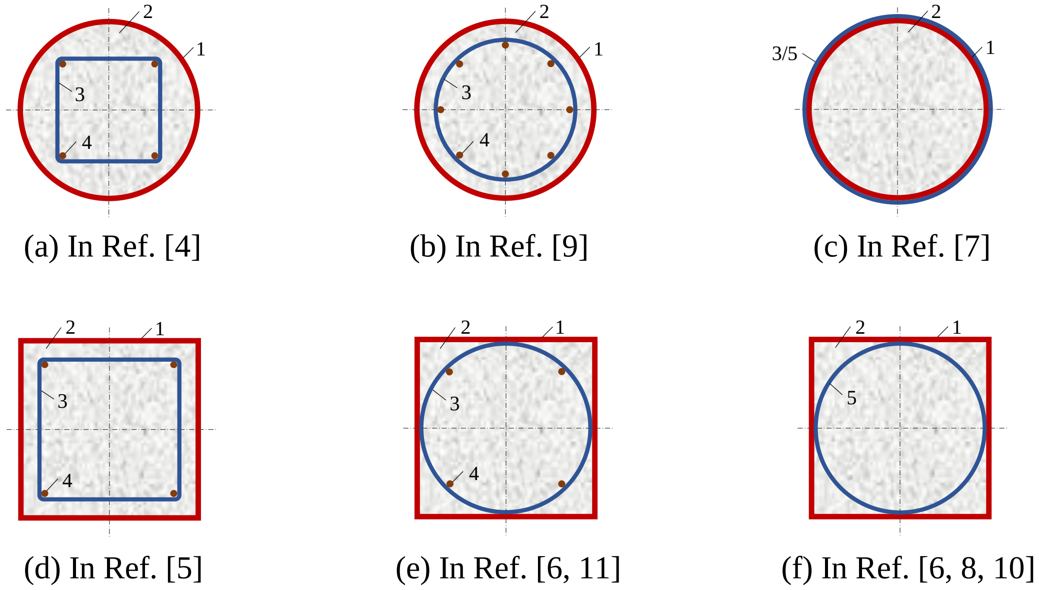

Fig. 1. Typical cross-section of the reinforced CFST in the literature.

(1−Steel tube; 2−Concrete; 3−Stirrups; 4−Longitudinal bar; 5−Spiral stirrup)

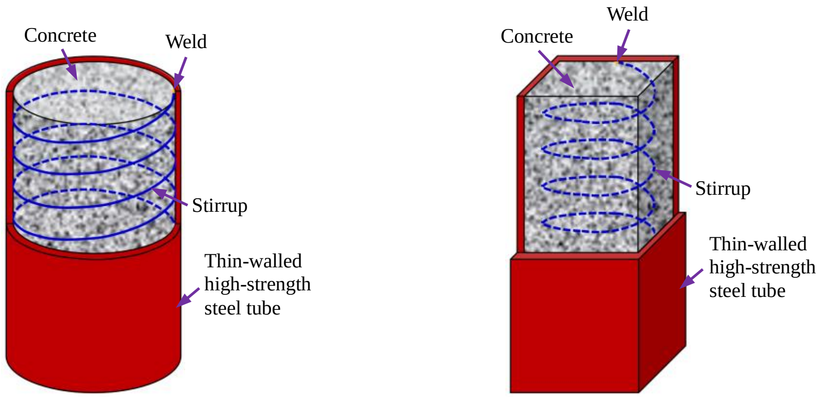

(a) Circular section   (b) Square section

Fig. 2. Schematic of CTHST with inner spiral stirrup.

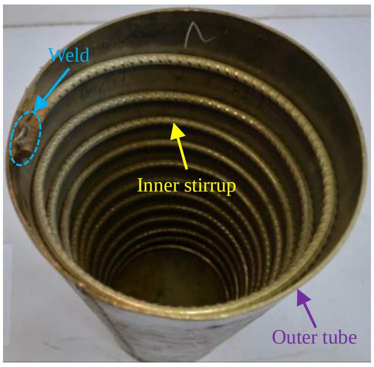

(a) Circular section

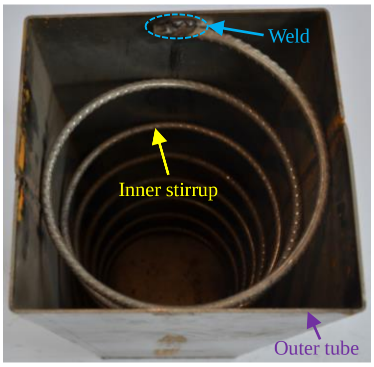

(b) Square section

Fig. 3. The finished outer tube and inner stirrup of the specimens.

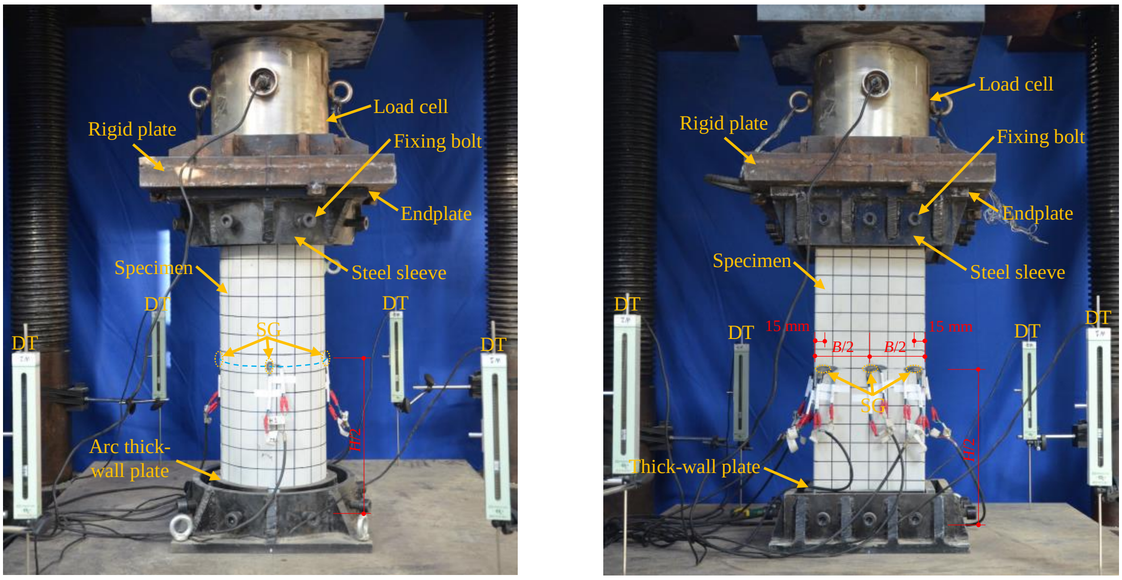

(a) Circular section (b) Square section

Fig. 4. Test set-up and measurement.

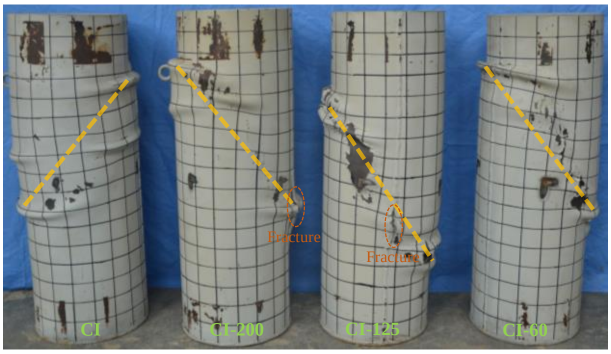

(a) Group CI

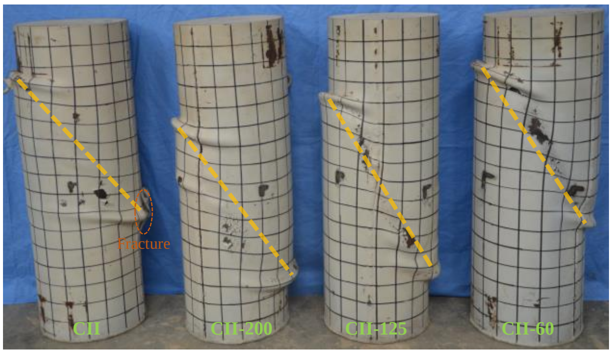

(b) Group CII

(c) Group SI

(d) Group SII

Fig. 5. Failure pattern of the specimens.

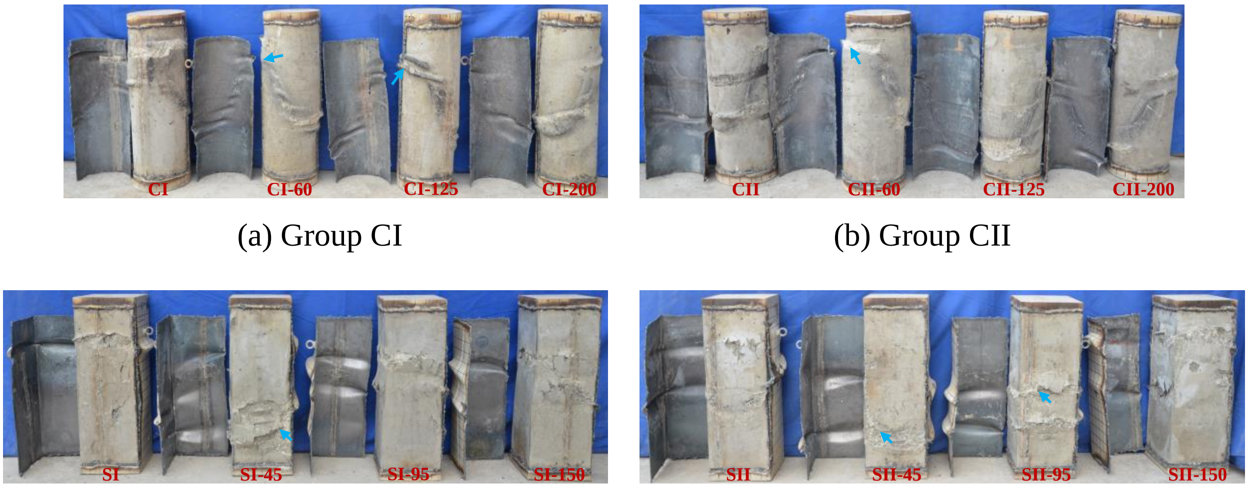

(a) Group CI
(b) Group CII
(c) Group SI
(d) Group SII

Fig. 6. Failure pattern of the concrete core.

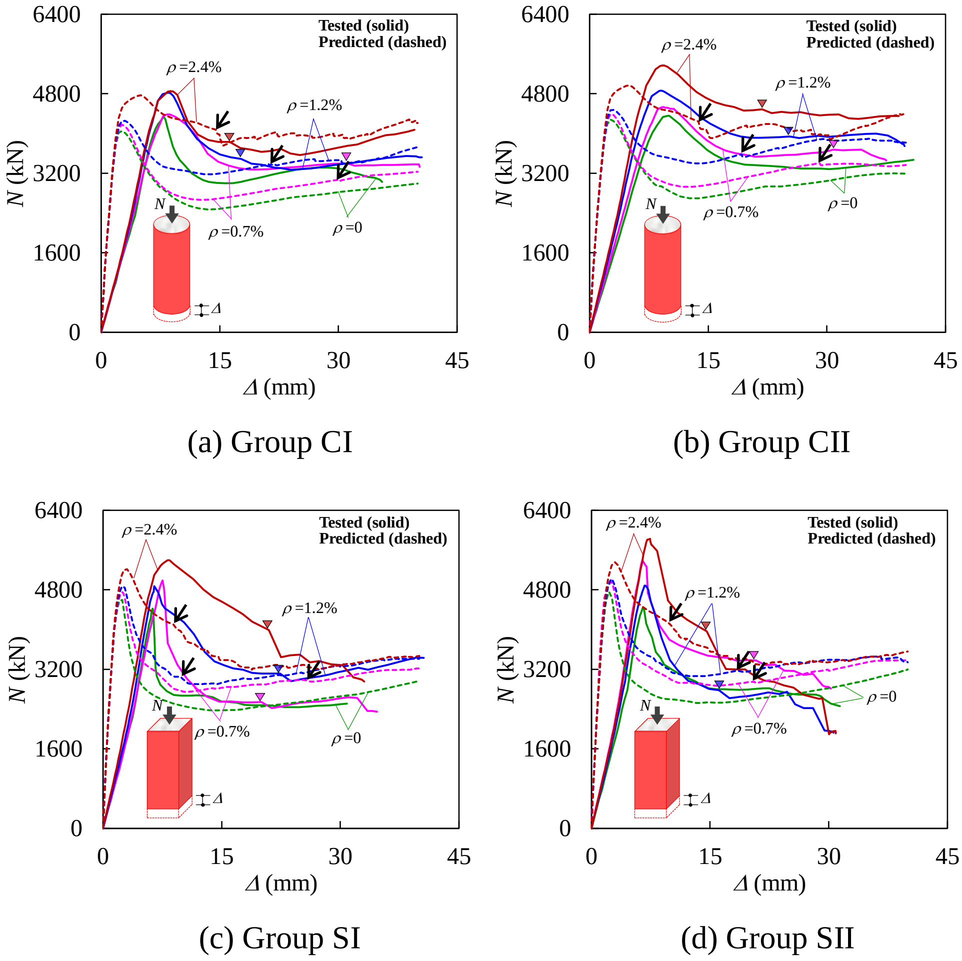

(a) Group CI

(b) Group CII

(c) Group SI

(d) Group SII

Fig. 7. Load (*N*) versus axial displacement (*Δ*) curve of the specimens.

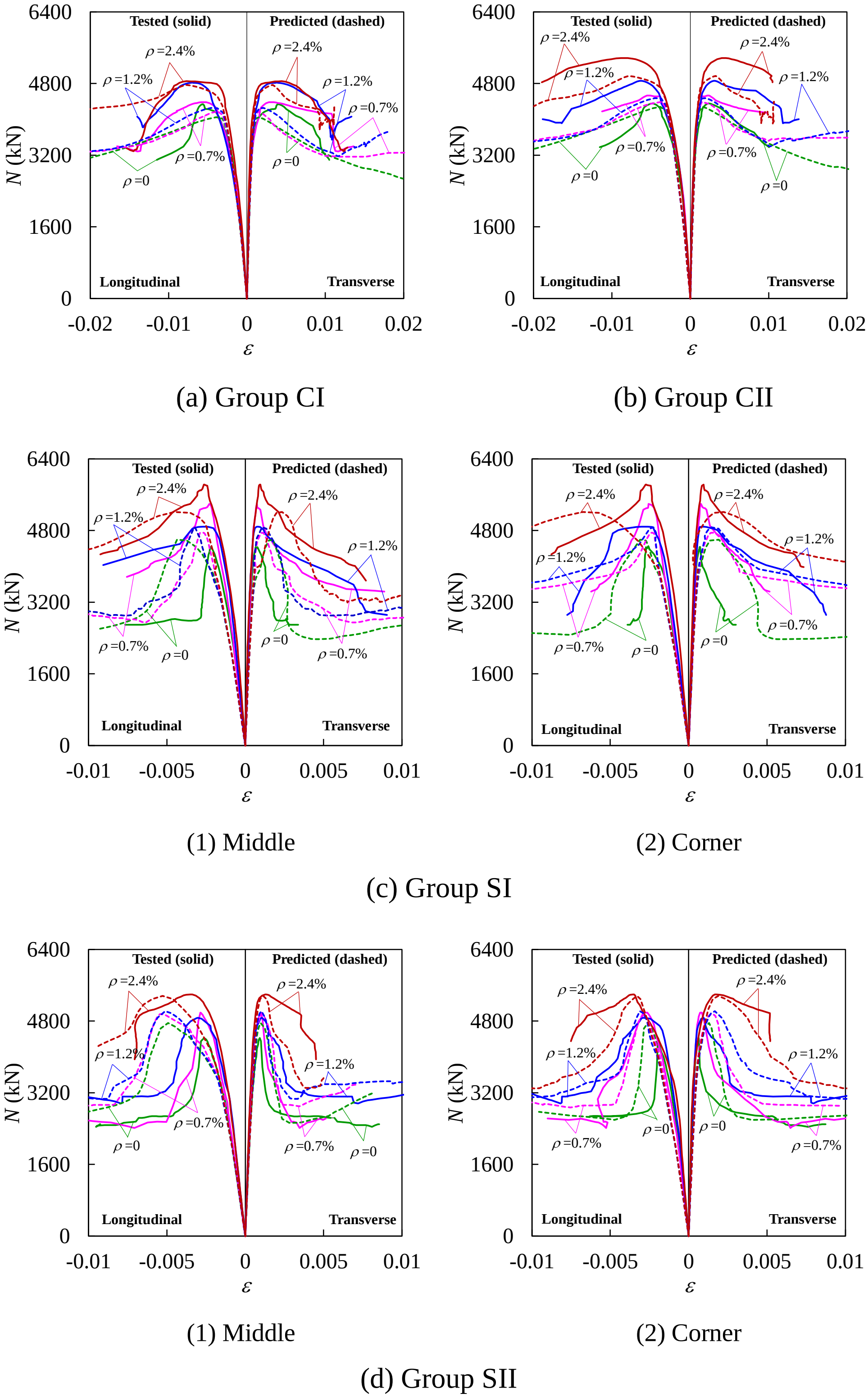

(a) Group CI

(b) Group CII

(1) Middle

(2) Corner

(c) Group SI

(1) Middle

(2) Corner

(d) Group SII

Fig. 8. Load versus strain relationship of the specimens.

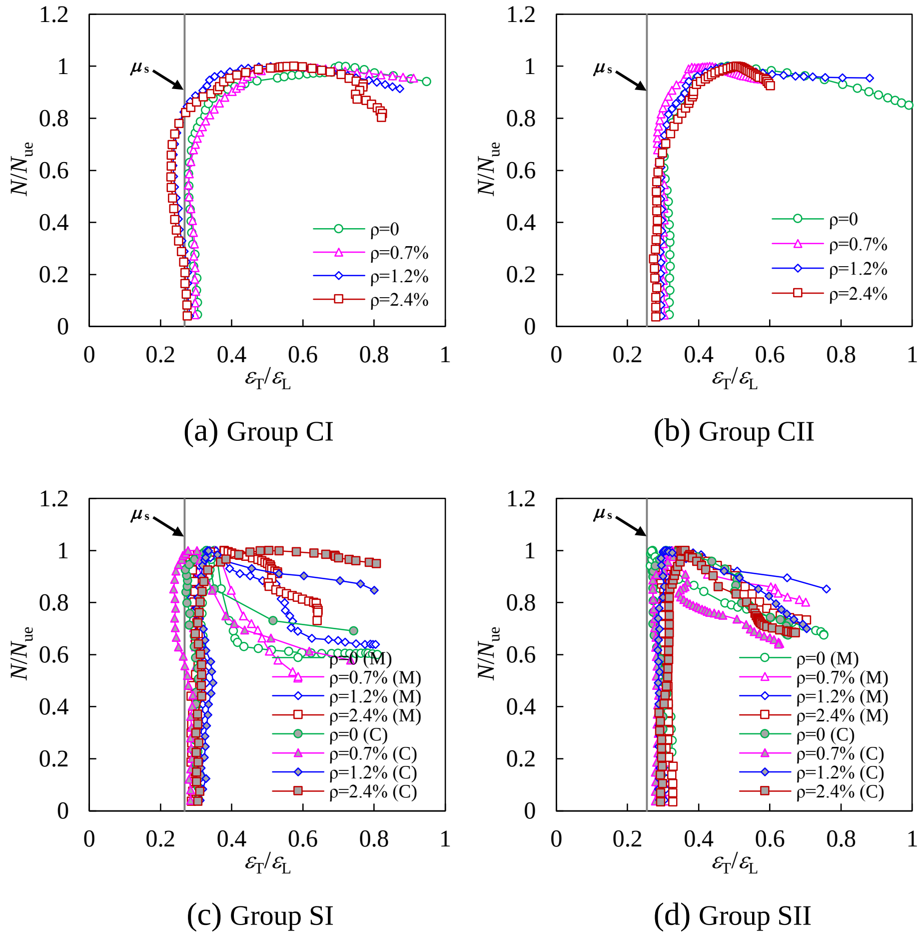

Fig. 9. Relationship between $\varepsilon_T/\varepsilon_L$ and N/N_{ue} of the specimens.

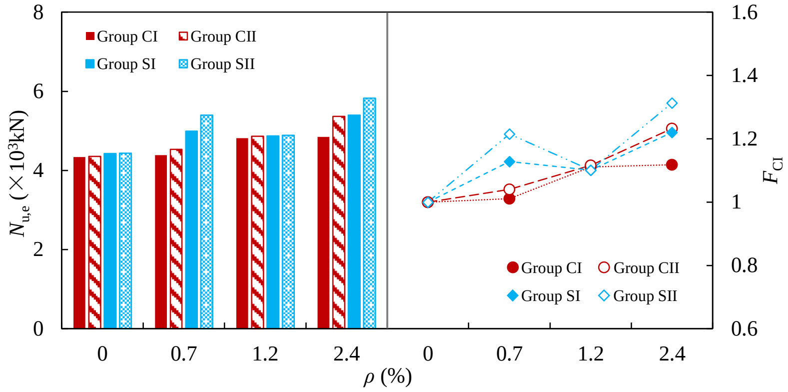

Fig. 10. Variation in the capacity (N_{ue}) and capacity improvement factor (F_{CI}) of the specimens.

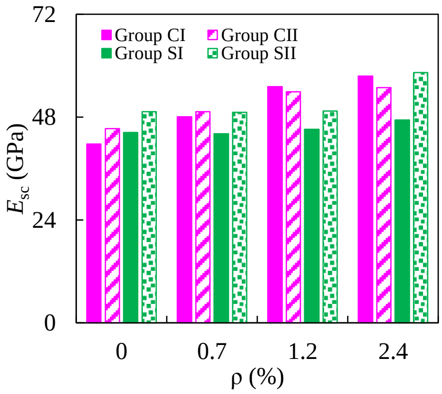

Fig. 11. Variation in the composite elastic modulus (E_{sc}) of the specimens.

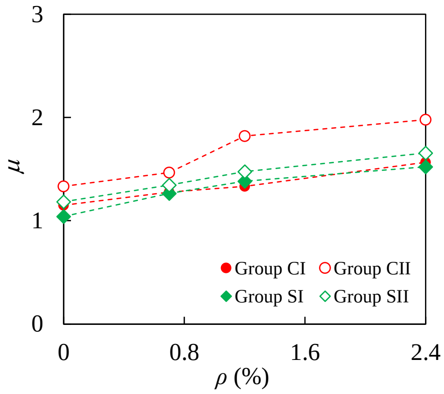

Fig. 12. Effect of parameters on ductility coefficient (μ) of the specimens.

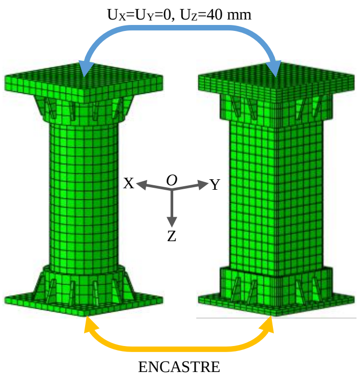

Fig. 13. Mesh division and boundary conditions of the FE model.

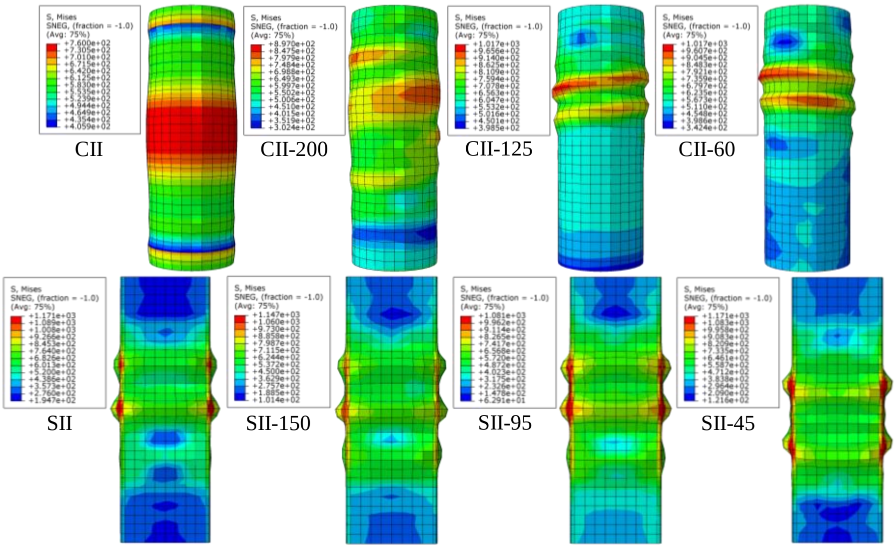

(a) Outer tube

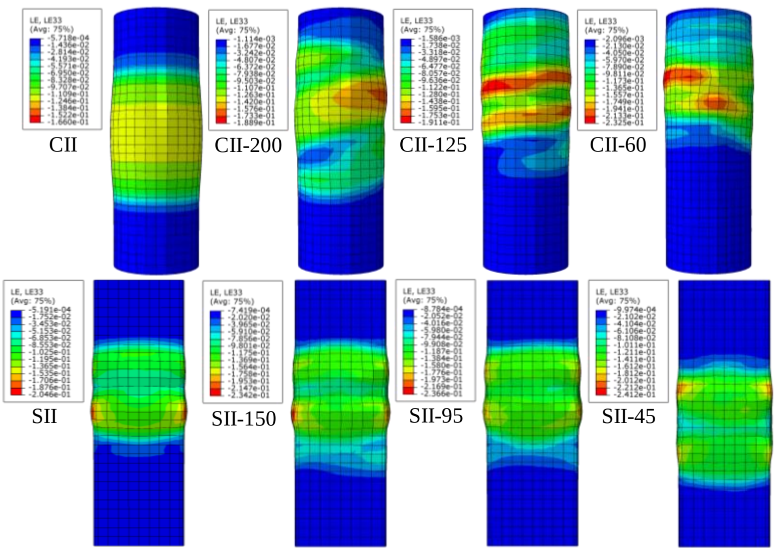

(b) Concrete core

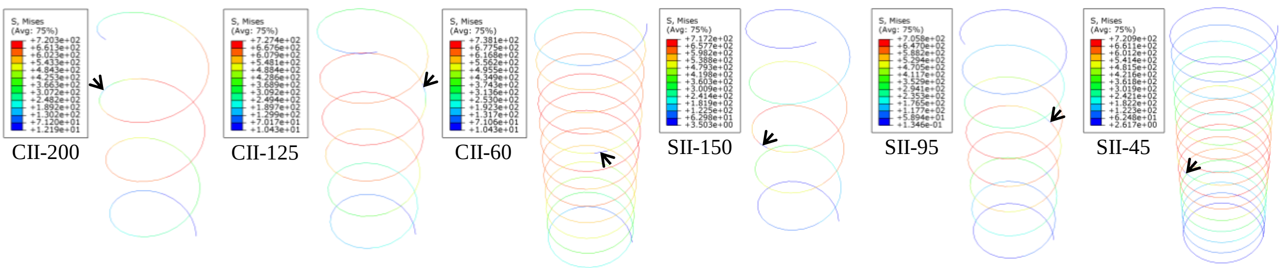

(c) Spiral stirrup with the first fracture

Fig. 14. The simulated failure patterns of typical specimens using the FE model.

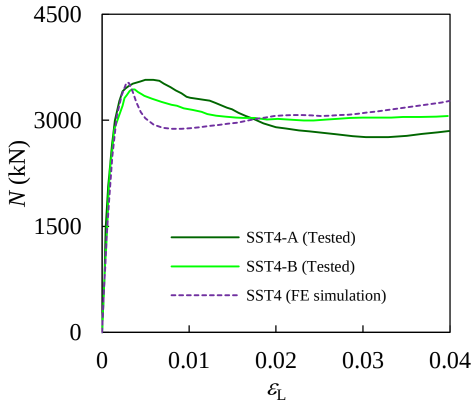

(a) SST4[6]

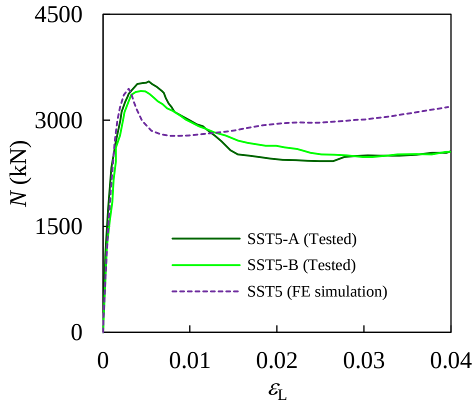

(b) SST5[6]

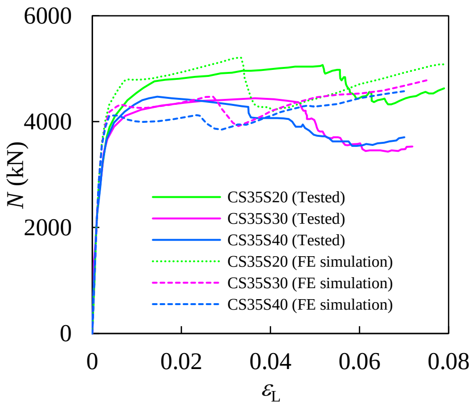

(c) Group CS35[10]

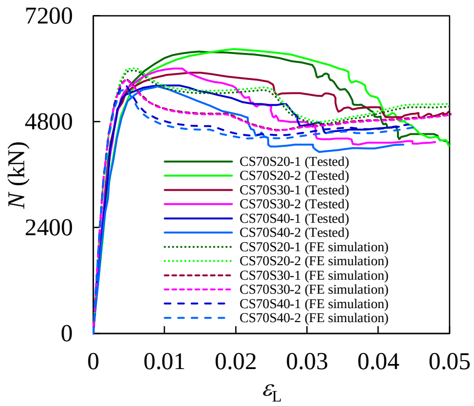

(d) Group CS70[10]

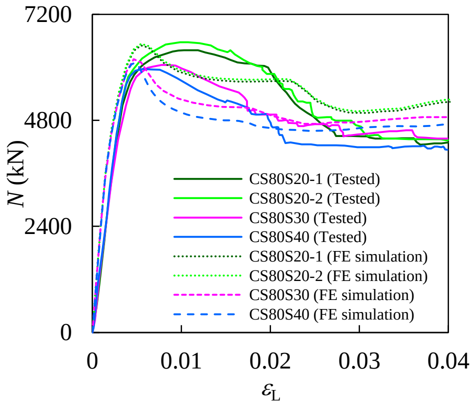

(e) Group CS80[10]

Fig. 15. Comparison between the simulated N-ε curves and the measured results in the literature.

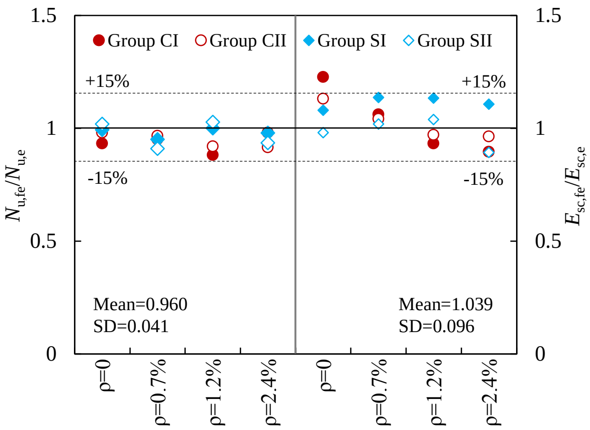

(a) Specimens in this paper

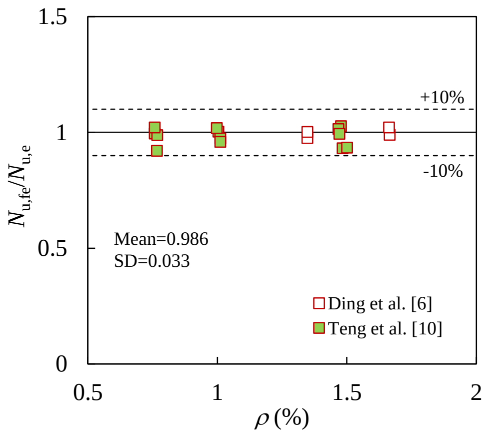

(b) Specimens in the literature

Fig. 16. Comparison between the predicted and measured mechanical indicators.

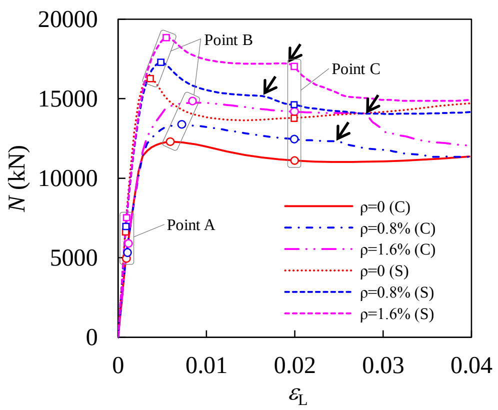

Fig. 17. $N-\varepsilon_{\mathrm{L}}$ curve of typical composite members.

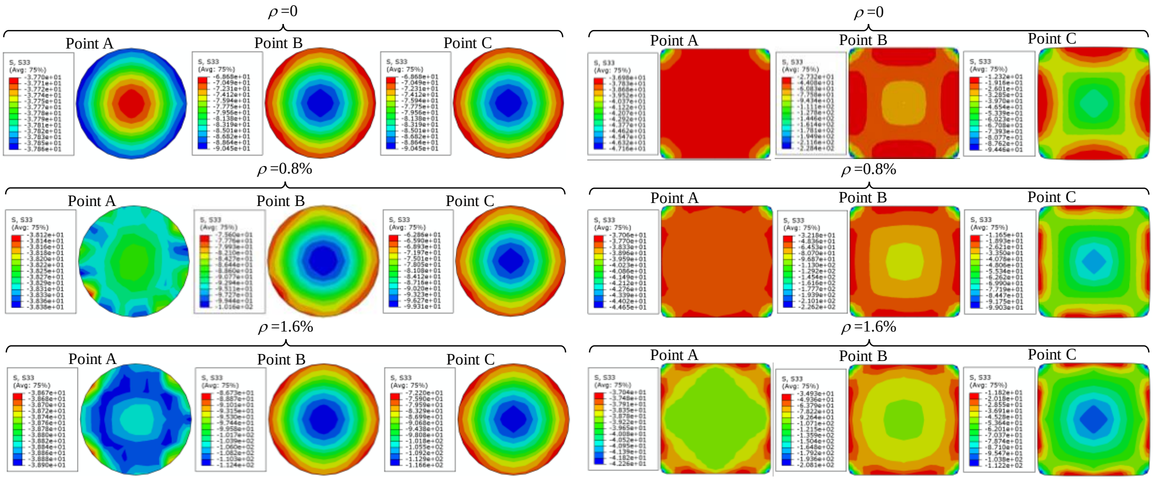

(1) Circular section (2) Square section

(a) Concrete core

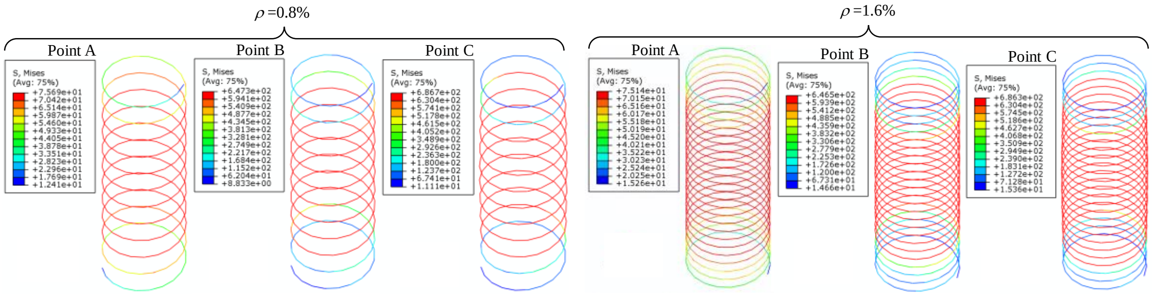

(1) Circular section

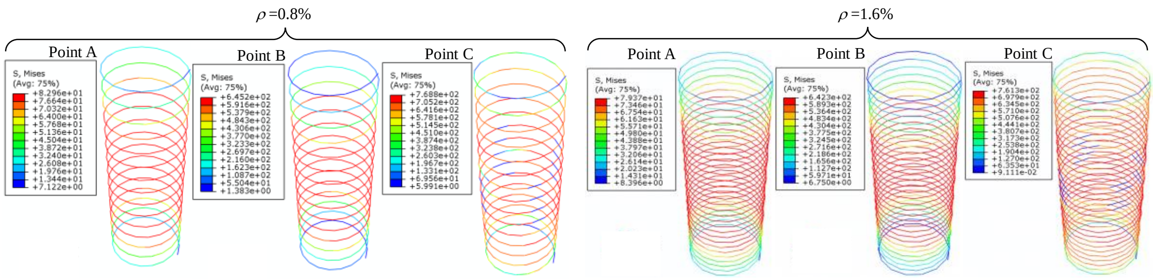

(2) Square section

(b) Spiral stirrup

Fig. 18. Stress state of the concrete core and spiral stirrup.

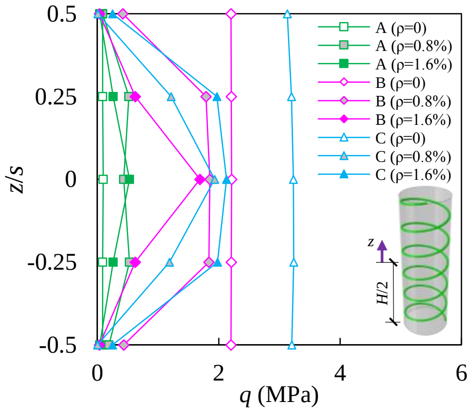

(a) Circular section

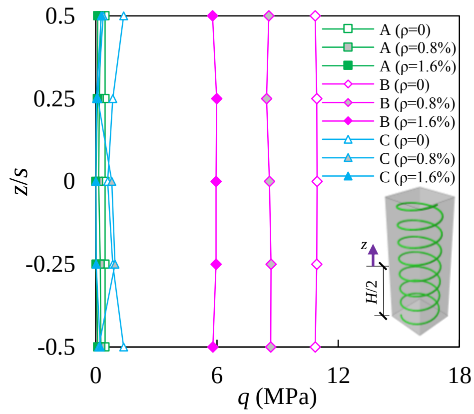

(b) Corner of square section

Fig. 19. Effect of ρ on the interaction stresses (q) between the steel tube and concrete core.

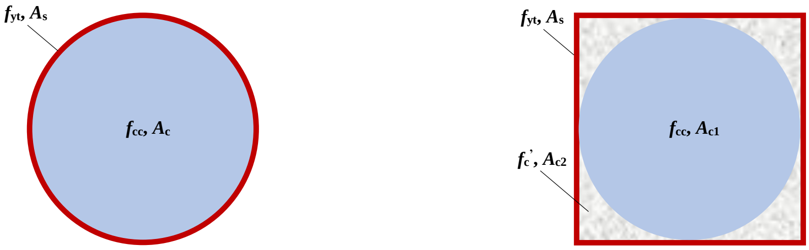

(a) Circular section (b) Square section

Fig. 20. Cross-section of the equivalent composite columns.

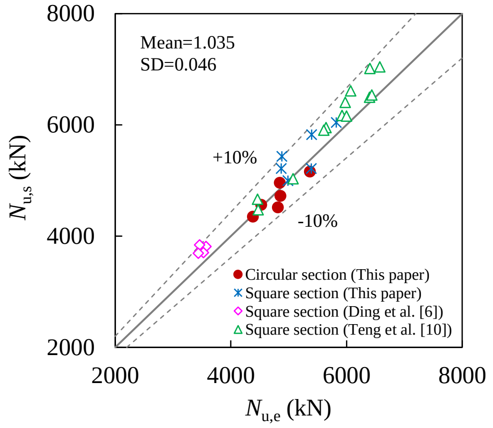

Fig. 21. Comparison between the simplified and experimental capacities.

Tables:

Table 1. Information of the specimens.

No.	Label	D (mm)	t (mm)	H (mm)	α_n	s (mm)	ρ (%)	f_{yt} (MPa)	f_{ys} (MPa)	f_{cu} (MPa)	$E_{sc,e}$ (GPa)	$E_{sc,fe}$ (GPa)	$E_{sc,fe}/E_{sc,e}$	$N_{u,e}$ (kN)	$N_{u,fe}$ (kN)	$N_{u,fe}/N_{u,e}$
1	CI	240	3.05	720	0.05	-	0	571.2	-	64.0	41.7	51.2	1.228	4338	4051	0.934
2	CI-200	240	3.05	720	0.05	200	0.7	571.2	639.3	64.0	48.1	51.1	1.062	4386	4175	0.952
3	CI-125	240	3.05	720	0.05	125	1.2	571.2	639.3	64.0	55.1	51.4	0.933	4820	4252	0.882
4	CI-60	240	3.05	720	0.05	60	2.4	571.2	639.3	64.0	57.6	51.6	0.896	4851	4760	0.981
5	CII	240	3.04	720	0.05	-	0	648.9	-	64.0	45.3	51.3	1.132	4357	4280	0.982
6	CII-200	240	3.04	720	0.05	200	0.7	648.9	639.3	64.0	49.3	51.4	1.043	4533	4390	0.968
7	CII-125	240	3.04	720	0.05	125	1.2	648.9	639.3	64.0	53.9	52.4	0.972	4861	4475	0.921
8	CII-60	240	3.04	720	0.05	60	2.4	648.9	639.3	64.0	54.9	53.0	0.965	5370	4921	0.916
9	SI	240	3.05	720	0.05	-	0	571.2	-	64.0	44.4	48.0	1.081	4425	4400	0.994
10	SI-150	240	3.05	720	0.05	150	0.7	571.2	639.3	64.0	44.1	50.2	1.138	4992	4754	0.952
11	SI-95	240	3.05	720	0.05	95	1.2	571.2	639.3	64.0	45.2	51.3	1.135	4873	4876	1.001
12	SI-45	240	3.05	720	0.05	45	2.4	571.2	639.3	64.0	47.3	52.4	1.108	5397	5289	0.980
13	SII	240	3.04	720	0.05	-	0	648.9	-	64.0	49.3	48.4	0.982	4438	4528	1.020
14	SII-150	240	3.04	720	0.05	150	0.7	648.9	639.3	64.0	49.1	50.1	1.020	5396	4915	0.911
15	SII-95	240	3.04	720	0.05	95	1.2	648.9	639.3	64.0	49.4	51.4	1.040	4886	5023	1.028
15	SII-45	240	3.04	720	0.05	45	2.4	648.9	639.3	64.0	58.4	52.2	0.894	5827	5454	0.936

Table 2. Properties of steel.

Type	Label	t/d_s (mm)	Yield strength (MPa)	Tensile strength (MPa)	Elastic modulus ($\times 10^5$N/mm^2)	Poisson's ratio	Elongation after fracture (%)
Tube	I	3.05	571.2	674.7	2.12	0.268	8.51
	II	3.04	648.9	754.2	2.07	0.255	7.62
Stirrup	/	8.78	639.3	742.9	1.93	/	4.27

Table 3. Mix proportion and properties of concrete

Mix proportion (kg/m³)						Properties				
Cement	Fly ash	Fine aggregate	Coarse aggregate	Water	WRA*	$f_{cu,28}$ (MPa)	f_{cu} (MPa)	E_c (GPa)	Slump (mm)	Spread (mm)
420	130	800	832	189.5	6.88	51.8	64.0	34.9	265	565

*WRA=water reducing admixture.